Component-wise analysis of laminated structures by hierarchical refined models with mapping features and enhanced accuracy at layer to fiber-matrix scales

Component-wise analysis of laminated structures by hierarchical refined models with mapping features and enhanced accuracy at layer to fiber-matrix scales

E. Carrera*, A.G. de Miguel †, A. Pagani‡

Mul^2 Group, Department of Mechanical and Aerospace Engineering,
Politecnico di Torino,
Corso Duca degli Abruzzi 24, 10129 Torino, Italy.

Abstract

Modern methodologies for the analysis of composite structures are demanded to satisfy the accuracy requirements at different scales, from micro to macro and possibly in a global/local sense. In this domain, the present paper proposes a hierarchical, component-wise approach for the linear static analysis of layered structures. By employing the Carrera Unified Formulation and a variational statement, finite element arrays of refined beam models are expressed in terms of fundamental nuclei. Legendre-based polynomials are utilized to implement, in a hierarchical form, higher-order beam kinematics. Also, curved cross-section geometries are formulated in a correct and consistent manner through mapping blending functions. Mapping and refined kinematics beam models are, thus, inherently combined to give the component-wise method, according to which each component of the structure (e.g., layer, fibres, and matrix) is modeled independently and with its geometric and mechanical characteristics. This approach is demonstrated to provide enhanced accuracy for the analysis of composite structures, from layer scale to fibre-matrix level, but still with low computational costs.

Keywords: Refined beam theories, Finite element method, Carrera unified formulation, Hierarchical Legendre expansions, Blending functions, Laminated structures, Fiber-reinforced composites, Global-local methods.

*Professor of Aerospace Structures and Aeroelasticity, e-mail: erasmo.carrera@polito.it
†Marie Curie PhD Student, e-mail: alberto.garcia@polito.it
‡Research Assistant, e-mail: alfonso.pagani@polito.it

1 Introduction

Composite materials have been increasingly employed during the last decades for the introduction of novel structural components in all types of engineering fields, specially in the aerospace. The advantages of laminated composite structures in terms of specific stiffness and strength in comparison with traditional metal alloys are widely known, see for instance the book of Reddy [1], and many aerospace companies are employing these advanced materials in major structural parts of their latest products. However, in order to fully exploit the capabilities of composites there are still many problems that need to be addressed, such as the correct understanding of failure, damage or fatigue, among others. A proper research of these problems goes through the development of enhanced modeling techniques that aim to capture the complex phenomena that is involved in the mechanical behavior of composites at different scales, from the macro-structure to the fiber-matrix scale, in the most efficient manner. This paper proposes a novel method for the global-local analysis of fiber-reinforced laminated structures based on the use of refined beam models.

A common practice for the stress analysis of composite structures is the use of 3D finite elements to mesh in detail all the different components to a desired level of accuracy. Nevertheless, the size of the computational problem is a limiting factor of solid analysis due to the several scales that play a role in the behavior of these materials. Many efforts have been focused on the development of efficient methods for the accurate analysis of composites with acceptable computational costs. The literature is vast on enhanced 1D and 2D formulations for the analysis of laminated structures. A comprehensive review of these refined methods was presented by Kapania and Raciti [2, 3]. Some of the well-established methods for the analysis of laminates are: higher-order models [4, 5, 6, 7, 8, 9], trigonometric theories [10], zig-zag models [11, 12, 13, 14], mixed variational theories [15, 16] and layer-wise methods [17, 18, 19, 20, 21, 22, 23]. Many of the aforementioned refined methods provide highly accurate stress solutions at the layer level. However, their use is usually limited to the global structural analysis since they cannot deal with the phenomena involved at the fiber scale.

Multi-scale approaches provide a tool to study the damage and failure of composites, in which the local phenomena at the scale of the constituents affects the global behavior of the structure. Multi-scale methods are usually based in a decomposition of the structural problem in a global analysis at the macro-scale, and a micromechanical analysis at the constituent level. Over the years, different micromechanical theories have been proposed and still nowadays there is a huge investment of resources in the field. Some of those methods are the self-consistent model [24], the Generalised Method of Cells (GMC) [25, 26, 27], the Mathematical Homogenization Theories (MHT) [28], the Representative Volume Element (RVE) [29, 30, 31] and the Mechanics of Structure Genome (MSG) [32]. Usually, the validity of the multi-scale approach relies on the accuracy of the micromechanical model. In this sense, one of the major concerns of the researchers remains to maintain the size of the micromechanical model under certain limits to make the study feasible in terms of computational efforts.

This paper presents a novel approach for the efficient global-local analysis of composite

structures based on the *Component-Wise* method and hierarchical advanced 1D models. The Component-Wise (CW) method can be defined as a modeling technique in which the different components of a composite are individually and independently modeled by means of a unique formulation. This methodology was devised in the framework of the Carrera Unified Formulation (CUF) in [33] for the analysis of composite laminates including layers, fibers and matrix, and then extended to the study of multi-component aircraft structures [34, 35], civil structures [36] and more recently for the evaluation of failure parameters in composites [37]. The CW method allows one to study the same structural problem using different scales. A particular laminated structure can be analyzed following global approach, i.e accounting for the properties of the homogenized layers, or at a local scale, i.e. selecting the components in which a detailed stress analysis is desired. Different beam theories can be employed to generate CW models. In this work, the Hierarchical Legendre Expansions (HLE) [38, 39] are used for the kinematic description of the cross-sectional domain. These models present some advantageous characteristics such as non-local expansion capabilities and hierarchical refinement of the beam kinematics, which make them an ideal tool for the CW analysis of composites. In addition, a novel mapping technique [40] for the cross-sectional expansions is used to capture the correct geometry of curved components, such as fibers, without the need of further refinements of the model and, therefore, optimizing the modeling phase.

The paper is organized as follows: first, a brief description of the 1D CUF formulation is provided in Section 2, with a focus on the HLE beam theories; then, the cross-sectional mapping technique is presented and a some insights about the CW-HLE modeling are highlighted; subsequently, the finite element approximation employed in this work is described in Section 3, with special attention to the derivation of the stiffness matrix in the form of fundamental nuclei; the numerical assessment of the proposed method can be found in Section 4; and finally, the main conclusions are drawn in Section 5.

2 CUF 1D theories

The high computational costs of solid models that are usually demanded for the accurate analysis of multi-component structures remains as one of the main limitations of the research field. As a consequence, the introduction of efficient models that can deal with the complex phenomena involved at multiple scales is of major importance. In this context, the Carrera Unified Formulation establishes a framework for the study and implementation of novel refined beam models that provide 3D-like solutions with great savings in computational costs. This section describes the main ideas of the CUF methodology and proposes a recent theory of structure for the global-local analysis of composites.

The Cartesian coordinate system adopted in this paper for a generic beam structure is illustrated in Fig. 1. The beam is placed along the y-axis in $0 \leq y \leq L$, whereas the cross-section, Ω, is described over the xz-plane. In the CUF framework, the generalized unknowns of the structural problem are expanded over the cross-section domain by arbitrary functions,

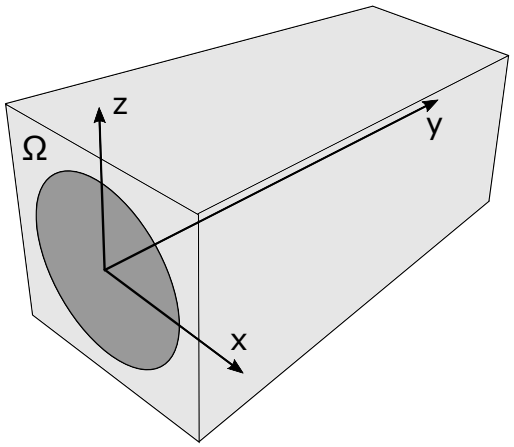

Figure 1: Coordinate reference frame.

as follows

$$\mathbf{u}(x, y, z) = F_\tau(x, z)\mathbf{u}_\tau(y) \quad \tau = 1, 2, ..., M, \tag{1}$$

where $\boldsymbol{u}(x,y,z)$ is the displacement vector, $F_\tau(x, z)$ corresponds to the expanding functions of the cross-section coordinates, and $\boldsymbol{u}_\tau(y)$ is the vector of the generalized displacements of the beam. The repeated subscript τ denotes summation and M is the total number of terms of the expansion. The choice of $F_\tau(x, z)$ and M is arbitrary and is introduced as an input of the model, defining the beam theory adopted. Since the introduction of the CUF, many beam theories of structure have been developed and applied to the analysis of compact, thin-walled, multi-component and composite structures, among others. Two of the most investigated 1D CUF models are the Taylor Expansions (TE) [9] and the Lagrange Expansions (LE) [41], although they are not described in this paper for the sake of brevity. The research activity of the present work is focused on the recently introduced Hierarchical Legendre Expansions (HLE) and its applications for the global-local analysis of composite materials.

2.1 Hierarchical Legendre Expansions (HLE)

The HLE theory of structure makes use of hierarchical sets of Legendre-based polynomials to expand the mechanical variables over the cross-section coordinates. The model was first introduced by Carrera *et al.* [38] and then extended to the layer-wise analysis of laminated structures by Pagani *et al.* [39]. Its main features include: the hierarchical structure of the beam kinematics, which is inspired in the definition of the 2D set of interpolation polynomials of the work of Szabò and Babuska [42]; and the dislocation of the expansion domains above the cross-section. These characteristics make HLE beam models a suitable candidate for the accurate analysis of structures that feature heterogeneities in the xz-plane, as the one shown in Fig. 1. The set of Legendre-based polynomials employed in the model are included in Fig. 2. They can be classified in vertex, side and internal expansions, which are described in the following.

- Vertex expansions: analogue to the bi-linear Lagrange polynomials. They are defined

as follows:

$$F_\tau = \frac{1}{4}(1 - r_\tau r)(1 - s_\tau s) \qquad \tau = 1, 2, 3, 4, \tag{2}$$

where r and s vary over the natural domain between -1 and $+1$, and r_τ and s_τ represent the vertex location in the natural system of coordinates.

- Side expansions: introduced for $p \geq 2$, where p is the polynomial order and, consequently, defines the beam theory approximation. They are null at all edges of the domain but one, being their expressions:

$$F_\tau(r, s) = \frac{1}{2}(1 - s)\phi_p(r) \qquad \tau = 5, 9, 13, 18, ... \tag{3}$$

$$F_\tau(r, s) = \frac{1}{2}(1 + r)\phi_p(s) \qquad \tau = 6, 10, 14, 19, ... \tag{4}$$

$$F_\tau(r, s) = \frac{1}{2}(1 + s)\phi_p(r) \qquad \tau = 7, 11, 15, 20, ... \tag{5}$$

$$F_\tau(r, s) = \frac{1}{2}(1 - r)\phi_p(s) \qquad \tau = 8, 14, 16, 21, ..., \tag{6}$$

where ϕ_p are the one-dimensional Legendre-type internal polynomials, as described in [42, 38], for instance.

- Internal expansions: included for $p \geq 4$, they vanish at all the edges of the quadrilateral domain. In total, there are $(p-2)(p-3)/2$ internal polynomials. For the sake of clarity, the three internal expansions correspondent to the sixth-order model are written here:

$$F_{28}(r, s) = \phi_4(r)\phi_2(s) \tag{7}$$

$$F_{29}(r, s) = \phi_3(r)\phi_3(s) \tag{8}$$

$$F_{30}(r, s) = \phi_2(r)\phi_4(s). \tag{9}$$

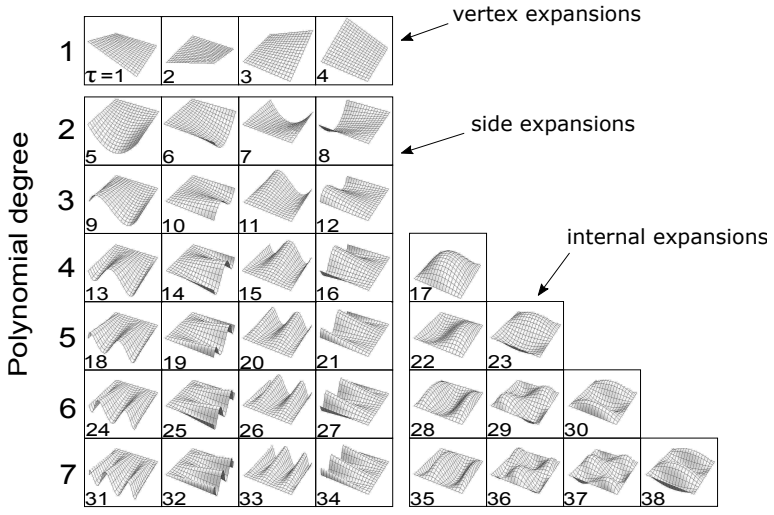

Figure 2: Linear to seventh-order, hierarchical Legendre-type expansion polynomials used for HLE beam models.

In HLE beam theories, the accuracy of the model is controlled by the polynomial order of the expansion, that is introduced in the analysis as an user input. The kinematics enrichment procedure can be easily explained with the support of Fig. 2: the first order model, denoted to as HL1, employs only the vertex expansions (first row); the second order model, HL2, adds the first 4 side expansions (second row); the third-order model incorporates other four expansions (third row) in a hierarchical manner; and so for the higher-order models. In this manner, the seventh-order model, HL7, includes all the polynomials shown in Fig. 2 for the formulation of the beam kinematics. Refined beam theories exploiting step-wise higher-order expansions of the displacement field can be implemented by dividing the cross-section domain in different sub-domains, each of which with its own HLE approximation, geometry, and material heterogeneity, in case. It is clear that, due to the high polynomial orders employed for the kinematics, the discretization of the physical domain of the cross-section should be coarse. Therefore, it is necessary to capture the correct shape of the structural components with a minimum number of segments, which leads to the introduction of advanced mapping techniques for the expansion domains.

2.2 Cross-sectional mapping

In HLE beam theories cross-sectional expansion sub-domains are large. The computation of the stiffness matrix terms requires the correct evaluation of the integrals of the expansion functions, F_τ, over the cross-section physical domain, Ω. So it comes necessary to accurately represent the curved boundaries of the sections with a reduced number of edges. The blending function method, introduced by Gordon and Hall [43], is an adequate approach to meet this demand. The main advanatge of this method is that it allows one to define the geometry of the physical surfaces, fibers and laminas for instance, independently of the kinematic refinement in a non-isoparametric sense. The technique here proposed is illustrated in this section, although a more detailed description of the different mapping techiques used for refined beam theories can be found in Pagani *et al.* [40].

The coordinates of a generic expansion domain in the global reference system are defined in the xz-plane through the mapping functions, $\mathbf{Q}$, as:

$$x = Q_x(r, s) \tag{10}$$

$$z = Q_z(r, s), \tag{11}$$

where r and s define in the natural plane of the quadrilateral domain. For illustrative purposes, first let us consider a domain with only one side curved, for instance side 2. The coordinates of this edge can be described by parametric functions of the type $x = x_2(s)$ and $z = z_2(s)$. The polynomial order of the parametrization can be chosen by the user depending on the

shape of the edges to be represented. For a third-order mapping, these functions read:

$$x_2(s) = a_x + b_x s + c_x s^2 + d_x s^3 \tag{12}$$

$$z_2(s) = a_z + b_z s + c_z s^2 + d_z s^3. \tag{13}$$

They are are defined in $-1 < (r, s) < 1$ so that $x_2(-1) = X_2$, $x_2(1) = X_3$, $z_2(-1) = Z_2$ and $z_2(1) = Z_3$, being (X_τ, Z_τ) the coordinates of the τ-th vertex of the quadrilateral domain in the global reference systems. The blending function method adds the geometrical description of the curved edge to the isoparametrical mapping functions, as follows:

$$x = Q_x(r, s) = F_\tau(r, s)X_\tau + \Big(x_2(s) - \big(\frac{1-s}{2}X_2 + \frac{1+s}{2}X_3\big)\Big)\frac{1+r}{2} \tag{14}$$

$$z = Q_z(r, s) = F_\tau(r, s)Z_\tau + \Big(z_2(s) - \big(\frac{1-s}{2}Z_2 + \frac{1+s}{2}Z_3\big)\Big)\frac{1+r}{2}, \tag{15}$$

where $\tau = 1, ..., 4$. The first term maps the quadrilateral straight domain through the vertex expansions, whereas the second accounts for the difference between the curve described by the parametric functions, $x_2(s)$ and $z_2(s)$, and the straight edge of the domain. This procedure can eventually be extended to all the edges of the expansion domain, resulting in the following mapping expressions:

$$x = Q_x(r, s) = \frac{1}{2}(1-s)x_1(r) + \frac{1}{2}(1+r)x_2(s) + \frac{1}{2}(1+s)x_3(r) \tag{16}$$

$$+\frac{1}{2}(1-r)x_4(s) - F_\tau(r, s)X_\tau \tag{17}$$

$$z = Q_z(r, s) = \frac{1}{2}(1-s)z_1(r) + \frac{1}{2}(1+r)z_2(s) + \frac{1}{2}(1+s)z_3(r) \tag{18}$$

$$+\frac{1}{2}(1-r)z_4(s) - F_\tau(r, s)Z_\tau. \tag{19}$$

In this manner, one can capture the exact shape of the integral domains above the cross-section of the beam and therefore nullify the geometrical error of the model. Figure 3 shows the application of the blending function method to the section of a generic fiber. The introduction of HLE beam models with mapping capabilities can be suitable for the accurate modeling of composites at several scales, such as laminates or fiber-reinforced structures, as described in the next section.

2.3 Component-Wise approach for the global-local analysis of composites

The multi-scale analysis of composite structures is dominated by the use of 3D brick elements for the representation of the geometry of the material constituents. However, the elevated number of layers, the different geometrical scales of the components or aspect ratio constrains of solid elements, can lead to prohibitive computational costs if accurate analysis are desired. The Component-Wise approach aims at alleviating this issue by modeling each component

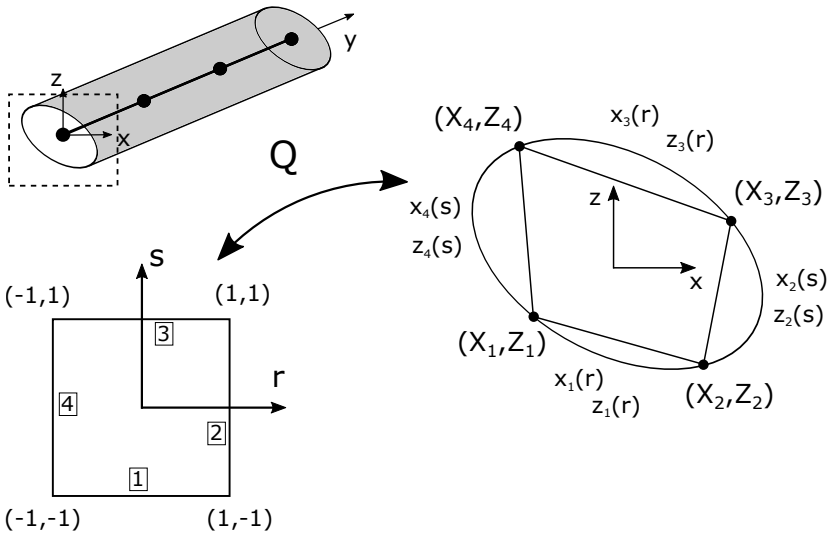

Figure 3: Mapping of a generic fiber cross-section by the blending function method.

of the composite by means of a refined 1D model. HLE beam theories can be employed to model the constituents (geometry and material properties) of a fiber-reinforced composite at different scales using a unique kinematic scheme. Homogenized parts, layers, fibers and matrices can be studied following a global-local approach, allowing the researcher to increase the accuracy of the model in the zones of interest while reducing the computational effort of the rest of the analysis. In addition, generic fibers can be modeled by means of a single HLE expansion (see Fig. 3) leading to an optimized computation of the stress fields in the fiber-matrix cells embedded in the analysis of the laminated structure. Figure 4 illustrates the different approaches that can be considered for the HLE modeling of composite materials, which are:

1. Equivalent Single Layer (ESL). The properties of the constituents are merged into one equivalent layer. The refinement of the model is controlled by the polynomial order of the HLE expansion and remains independent of the number of layers of the original composite. In ESL models, the continuity of the transverse stresses across the laminate and the piece-wise discontinuity of the displacements derivatives is generally not satisfied.

2. Layer-Wise (LW). Each layer is modeled independently using non-local HLE expansions and the continuity of transverse stresses is satisfied if high-order polynomials are used for the beam kinematics. It neglects the high gradients of the stresses at the fiber-matrix scale.

3. Component-Wise (CW). This approach gives the user the freedom to tune the accuracy of the analysis in two manners: first, by the description of the geometrical characteristics of the model (layers, fiber and matrix can be accounted in a unique formulation), and second, by the hierarchical enrichment of the kinematics through the HLE expansion order in desired areas of the problem domain.

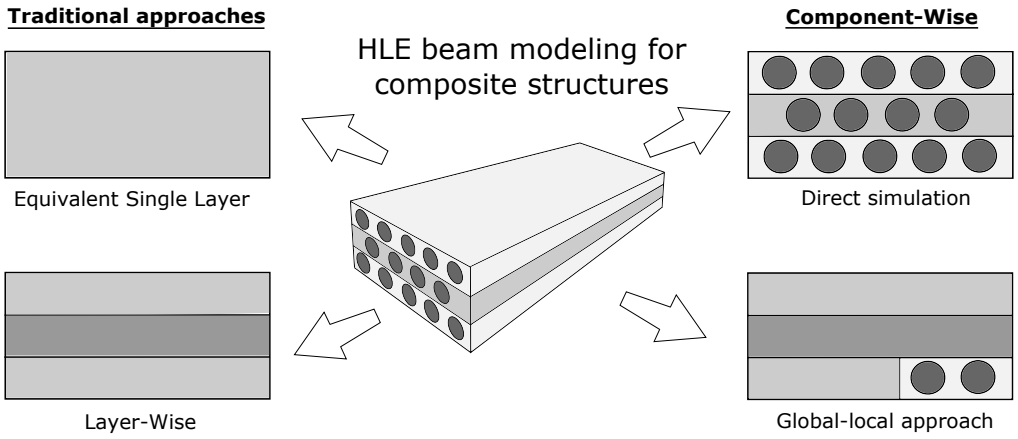

Figure 4: HLE beam analysis of composite materials: modeling approaches.

On the right-hand side of Fig. 4, the reader can observe two possible simulation approaches for the CW analysis of a laminated structure. One accounts for the fibers and matrix of each layer, and other follows a global-local approach including homogenized layers, some fibers and the surrounding matrix. The focus of the present work is about the use of HLE beam theories for the development of LW and CW models. Although the ESL approach is described here for the sake of completeness, it is not considered for the numerical assessments.

3 Finite element formulation

In this work, the Finite Element Method (FEM) is used solve the structural problem in the framework of CUF. The generalized displacements unknowns, $\mathbf{u}_\tau$, are interpolated over the beam axis by means of classical FEM shape functions, N_i, as:

$$\mathbf{u}_\tau(y) = N_i(y)\mathbf{u}_{\tau i}, \qquad i = 1, 2, ..., n, \tag{20}$$

where $\mathbf{u}_{\tau i} = \{u_{x_{\tau i}} \; u_{y_{\tau i}} \; u_{z_{\tau i}}\}^T$ is the nodal unknown vector and n is the number of nodes per element. Now, introducing the FEM approximation of Eq. 20 into the CUF kinematics of Eq. 1, one obtains the following displacement field:

$$\mathbf{u}(x, y, z) = F_\tau(x, z)N_i(y)\mathbf{u}_{\tau i}. \tag{21}$$

Four-node Lagrangian 1D elements are used in this paper to discretize the beam axis, which lead to a cubic approximation of the unknown variables along the y-coordinate. For a more detailed description of the FEM applications of CUF, the reader is referred to Carrera *et al.* [44]. It is important to note that the choice of the theory of structure (TE, LE, HLE) and the kinematics (i.e. discretization of the cross-section and polynomial order of the expansion) are independent of the finite element discretization employed to solve the governing equations.

It is of common knowledge that beam elements, as well as other FEM formulations, are prone to suffer from shear locking, specially in bending-dominant problems when thin struc-

tures are considered. Many different methods can be found in the literature that mitigate this numerical issue. Among those, the reduced integration schemes [45, 46] might be the most widely spread. In the present work, the MITC method [47, 48] is employed in all numerical cases to eliminate the detrimental effects of the shear locking and to obtain highly accurate solutions for the shear components of the stress field. This capability remains of major importance for the correct understanding of the complex phenomena that occur in composite materials at the fiber scale. For more details about the implementation of the MITC method on refined beam theories, interested readers are referred to Carrera *et al.* [49].

3.1 Fundamental nucleus of the stiffness matrix

The problem arrays, i.e. stiffness matrix and loading vector, are obtained via the principle of virtual displacements. For linear static analysis, it reads

$$\delta L_{int} = \int_L \int_\Omega \delta \boldsymbol{\varepsilon}^T \boldsymbol{\sigma} \, d\Omega \, dy = \delta L_{\text{ext}}, \tag{22}$$

where δL_{int} is the virtual variation of the strain energy and δL_{ext} corresponds to the virtual variation of the work of the external loads. L is the length of the beam and Ω is the surface of the cross-section. In this work, the strain vector, $\boldsymbol{\varepsilon}$, is related to the displacements through the 3D linear geometrical relation, whereas the stress vector, $\boldsymbol{\sigma}$, is obtained through the constitutive equations. Using these definitions and introducing the displacement field of Eq. 21, the virtual variation of the strain energy can be rewritten as

$$\delta L_{\text{int}} = \delta \mathbf{u}_{\tau i}^T \mathbf{K}^{\tau s i j} \mathbf{u}_{s j}, \tag{23}$$

where $\mathbf{K}^{\tau s i j}$ is the *fundamental nucleus* of the stiffness matrix. This array has a 3×3 arrangement and contains the basic information of the structural model. For illustrative purposes, a diagonal and an out-of-diagonal components of the fundamental nucleus are provided in the following for the case of transversely isotropic materials with arbitrary orientations in the xy-plane (e.g. fiber-reinforced laminae).

$$\begin{aligned}
K_{xx}^{\tau s i j} &= \widetilde{C}_{22} \, I_{ij} \, E_{\tau,x \, s,x} + \widetilde{C}_{44} \, I_{ij} \, E_{\tau,z \, s,z} + \widetilde{C}_{26} \, I_{ij,y} \, E_{\tau,x \, s} + \widetilde{C}_{26} \, I_{i,y \, j} \, E_{\tau s,x} + \widetilde{C}_{66} \, I_{i,y \, j,y} \, E_{\tau s} \\
K_{xy}^{\tau s i j} &= \widetilde{C}_{23} \, I_{ij,y} \, E_{\tau,x \, s} + \widetilde{C}_{45} \, I_{ij} \, E_{\tau,z \, s,z} + \widetilde{C}_{26} \, I_{ij} \, E_{\tau,x \, s,x} + \widetilde{C}_{36} \, I_{i,y \, j,y} \, E_{\tau s} + \widetilde{C}_{66} \, I_{i,y \, j} \, E_{\tau s,x}.
\end{aligned} \tag{24}$$

It can be easily demonstrated that the other seven terms of the fundamental nucleus can be obtained by permutations from Eq. 24, see [50]. In Eq. 24, the terms I_{ij}, $I_{ij,y}$, $I_{i,yj}$, and $I_{i,y\,j,y}$ refer to the integrals of the shape functions along the y-axis, e.g. $I_{ij,y} = \int_l N_i \, N_{j,y} \, \mathrm{d}y$; whereas the E terms refer to the integrals of the transverse expansions above the cross-section surface, such as for example $E_{\tau,x \, s,z} = \int_\Omega F_{\tau,x} F_{s,z} \, d\Omega$. The comma indicates partial derivation with respect to the global coordinates x, y and z. All the integrals are computed numerically

by means of the Gauss-Legendre quadrature. For the sake of brevity, the derivation of the loading vector is not included here, but it can be found in [44]. One can notice that, according to the notation here employed, any refined beam model can be straightforwardly generated by expanding the fundamental nucleus, $\mathbf{K}^{\tau sij}$, over τ, s, i and j.

4 Numerical results

Several numerical assessments are included in this section. First, the HLE models are employed to analyze a L-angle laminated beam using a pure layer-wise approach. Secondly, a comprehensive mechanical analysis is performed on fiber-matrix volumes, with a focus on the stress distributions over the section and fiber-matrix interface.. Finally, the Component-Wise method is exploited to study a cross-ply beam that includes fiber, matrix and equivalent layers. The numerical solutions are in all cases confronted against those from shell and solid elements generated in the commercial software MSC Nastran.

4.1 L-angle beam

The first numerical example, selected to test the capabilities of the proposed formulation in dealing with curved laminated structures, is an L-angle thin-walled beam composed of two plies of different metals. L-angle beams are often used for secondary structural applications, such as stiffeners or junctions, and their geometrical features make analyses with layer-wise accuracy usually computationally expensive. The length of the structural body is $L = 1$ m, and the cross-sectional geometry is represented in Fig. 5 (a), where $h_1 = 15$ mm is the dimension of both flanges, $t = 2$ mm is the total thickness of the laminate and $r = 5$ mm is the outer radius of the curvature of the angle. The slenderness ratio of the body is as high as $L/h = 50$. The two metallic plies have the same thickness and they are modeled as isotropic materials with the following characteristics: Young's modulus, E, equal to 75 GPa and Poisson's ratio, ν, equal to 0.33, for the inner ply; whereas $E = 200$ and $\nu = 0.29$ for the outer ply. The structure is clamped at one end and a vertical load of magnitude $F_z = -50$ N is applied at the top corner of the free-edge, corresponding to point A in Fig. 5 (a).

Figure 5 (b) shows the modeling procedure adopted for the HLE theories of structure with mapping capabilities. The cross-sectional surface is represented with six expansion domains, three per layer, with no geometrical loss of accuracy. A single HLE curved domain is used per each layer to describe the angle of the section. The accuracy of the model is then tuned by the polynomial order of the expansion functions, that is selected as an input of the analysis. The 1D finite element mesh consists of ten cubic (B4) MITC beam elements along the longitudinal axis. As discussed before, the introduction of the MITC formulation has the double purpose of eliminating the shear locking and computing the correct distribution of the transverse shear components, see [49]. Cubic MITC beam elements are used in all the assessments presented hereinafter.

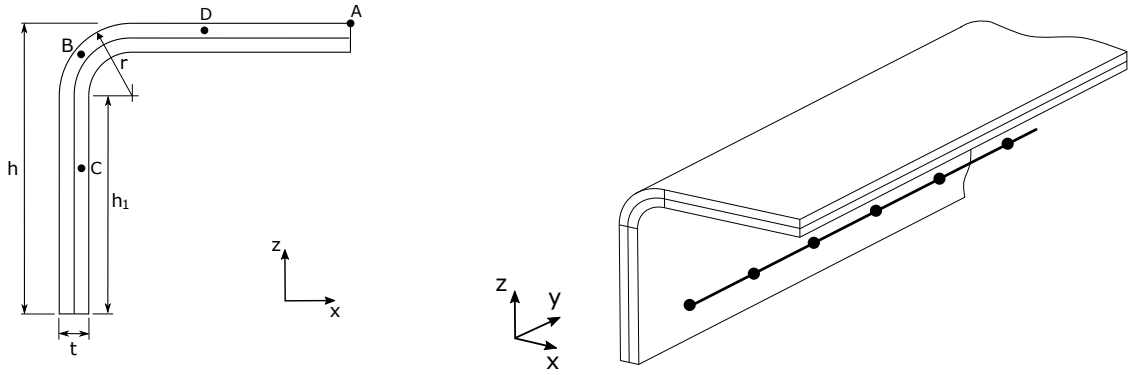

(a) Geometry of the cross-section

(b) 1D refined model

Figure 5: L-angle laminate structure.

Table 1 shows the results in terms of displacements and stresses of the L-angle laminate for an increasing order of the cross-sectional expansions, from quadratic to 8^{th} order. Solid and plate models have been generated using the commercial software MSC Nastran [51] and are used here as reference solutions. The 3D model makes use of 8-node brick elements (HEXA8) and it includes a distribution of four elements across the thickness per ply. On the other hand, two plate models of increasing number of 4-node plate elements (QUAD4) are included for convergence purposes, referring QUAD4_1 to the coarse one and QUAD4_2 to the refined one. The location of the solution points is indicated in Fig. 5 (a). The stress components are evaluated at the center of the layer in the thickness direction and points C and D are placed at the middle of the height and width, respectively.

Model	$u_x \times 10^2$ Point A	$u_y \times 10^4$ Point A	$u_z \times 10^2$ Point A	$\sigma_{yy} \times 10^{-8}$ Point B	$\sigma_{yz} \times 10^{-7}$ Point C	$\sigma_{xy} \times 10^{-6}$ Point D	DOFs
MSC Nastran solutions							
HEXA8	4.867	-3.750	-7.823	1.480	-1.025	9.738	232200
QUAD4_1	4.992	-4.736	-7.987	1.183	-2.170	20.275	43750
QUAD4_2	4.990	-4.734	-7.981	1.183	-2.146	20.044	161250
HLE beam models							
HL2	5.789	-6.789	-6.374	1.488	0.103	-0.486	2697
HL3	4.831	-3.730	-7.771	1.472	-1.029	9.784	4278
HL4	4.832	-3.731	-7.774	1.472	-1.007	9.581	6417
HL5	4.832	-3.731	-7.776	1.471	-1.019	9.698	9114
HL6	4.832	-3.731	-7.778	1.471	-1.039	9.883	12369
HL7	4.832	-3.731	-7.778	1.471	-1.028	9.780	16182
HL8	4.832	-3.731	-7.779	1.471	-1.027	9.769	20553

Table 1: Results in terms of displacements [m] and stresses [Pa] for the L-angle laminated beam. The displacements are evaluated at $y = L$, whereas the stresses at $y = L/2$.

To complete the assessment of the accuracy of the stress solutions obtained from HLE beam models, Figs. 6, 7 and 8 show the distribution of longitudinal, σ_{yy}, and shear, σ_{yz} and σ_{xy}, stresses over the surface of the section at midspan cross-section. In Figs. 6(a),

7(a) and 8(a), the reader can find the plots of these stress components across the thickness of the laminate at the location of the evaluating points (B, C and D, respectively). The solid (HEXA8) and plate ($QUAD4_2$) solutions are also included in the graphs for comparison purposes. The following comments can be made on the basis of the results obtained:

- According to the solutions of Table 1, it is possible to state that the HLE beam models provide acceptable solutions already for the third order expansion (HL3), both in terms of displacements and stresses. The maximum relative error in comparison with the solid model is 0.66 %, corresponding to the vertical displacement, u_z. These results show that HLE beam models can deal not only with classical bending and torsional effects, but also more complex phenomena such warping and in-plane deformations with a 3D-like accuracy.

- While typical commercial plate elements only foresee constant distributions of strains and stresses across the laminate stack of plies (see $QUAD4_2$), HLE distributions show a 3D like accuracy in representing the stress distributions of the laminate, being in good agreement with the solid model (HEXA8) for all cases included in Fig. 6, 7 and 8. On the other hand, the computational costs in comparison with the solid model remain lower than 9 % in terms of degrees of freedom for all polynomial orders considered.

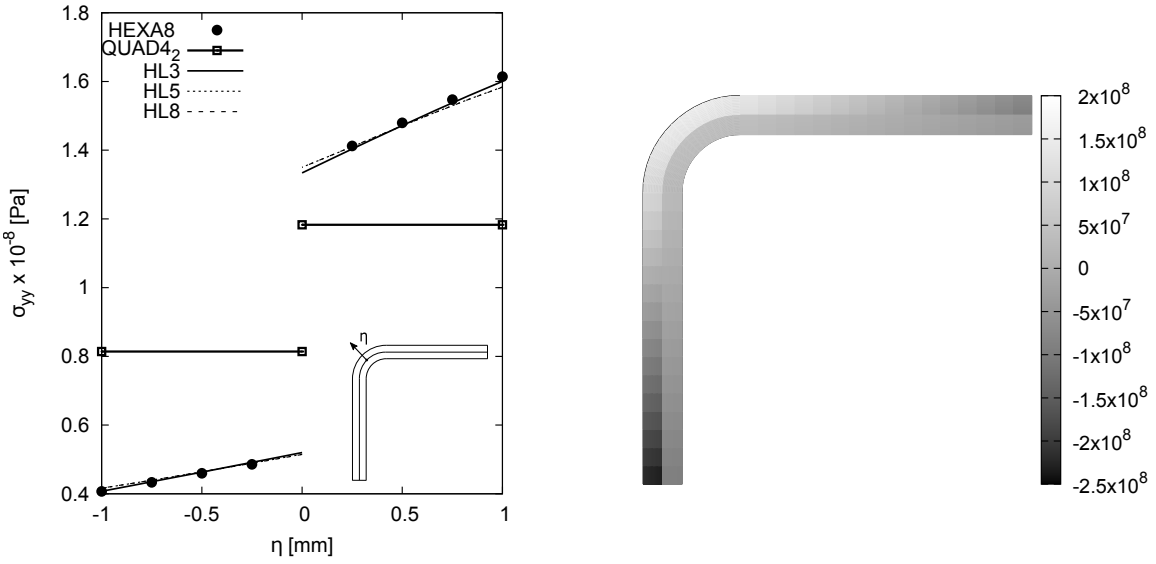

(a) σ_{yy} at point B

(b) surface plot

Figure 6: Distribution of longitudinal stresses, σ_{yy}, of the laminated beam at midspan.

4.2 Fiber-matrix analysis

As second numerical example, the capabilities of the HLE mapped models are employed to perform a structural analysis of a fiber-matrix cell at the micro-scale. The fiber is considered as cylindrical and the matrix is bounded around it conforming a square pack, as shown in

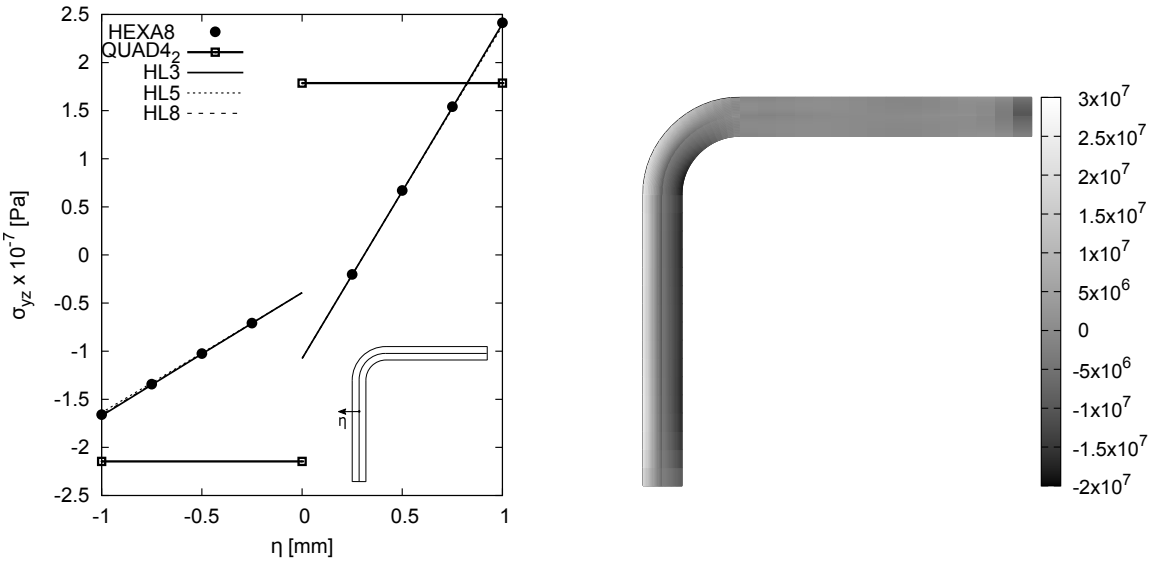

(a) σ_{yz} at point C (b) surface plot

Figure 7: Distribution of shear stresses, σ_{yz}, of the laminated beam at midspan.

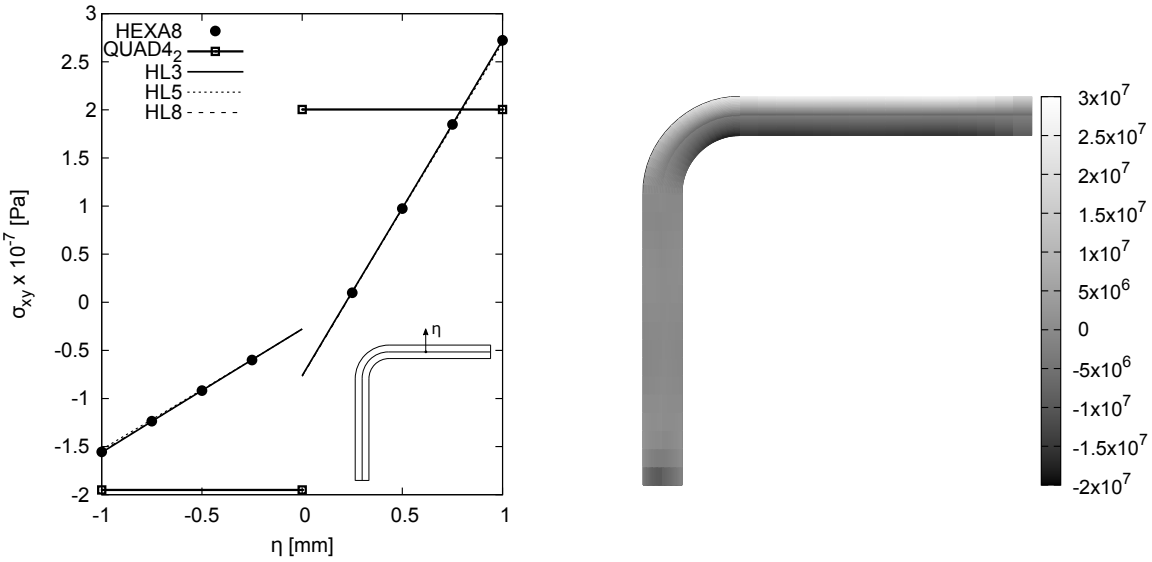

(a) σ_{xy} at point D (b) surface plot

Figure 8: Distribution of shear stresses, σ_{xy}, of the laminated beam at midspan.

Fig. 9 (a). The length of the body, L, is as high as 1 mm, whereas the diameter of the fiber, d, is equal to 0.08 mm and the total width of the section, b, is equal to 0.1 mm. Both components have been considered as isotropic materials for the sake of simplicity and with no loss of generality. For the fiber, the Young's modulus, E, is equal to 202.038 GPa and the Poisson ratio, ν, is equal to 0.2128, whereas for the matrix, $E = 3.252$ GPa and $\nu = 0.355$.

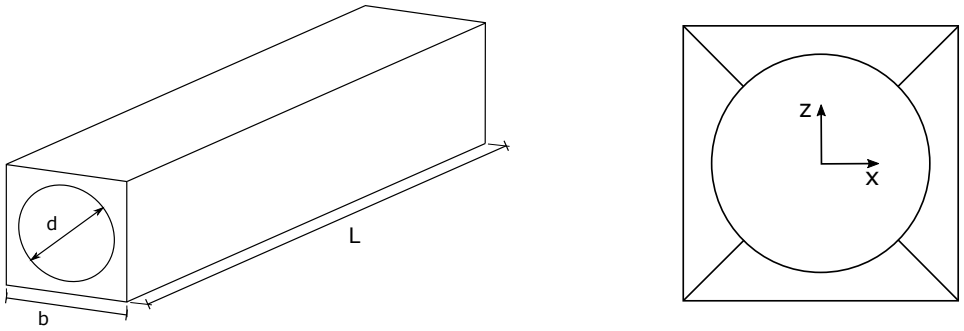

(a) Fiber-matrix beam geometry

(b) Cross-section HLE modeling

Figure 9: Fiber-matrix representative structure and cross-sectional domain subdivision for HLE beam models.

Fig. 9 (b) shows the cross-section domain discretization for the HLE beam model. One of the main advantages of the proposed approach for the study of fiber-reinforced structures at the micro-scale is the possibility of modeling the fibers using only one single HLE expansion with curved edges, allowing one to reduce greatly the complexity of the model while representing the correct geometry of each component. The accuracy of the analysis is then selected by the user by trimming the polynomial order of the theory of structure, without the need of iterative refinements of the domain discretization. For the numerical assessment, a clamped-free configuration is selected and a vertical point force of magnitude $F_z = -0.1$ N is applied at the center of the fiber at $y = L$. The longitudinal axis is discretized with ten cubic MITC beam elements, which, on the basis of analysis performed in previous works [49], provide convergent results in terms of the finite element mesh.

HLE beam solutions of vertical displacements and stresses at various points are included in Table 2, together with the number of degrees of freedom of each model. Results from the literature of the same study case, obtained from Taylor Expansions and Lagrange Expansions in Carrera *et al.* [33], are also included for comparison reasons. Three Nastran solid element solutions are used as references as well. These models have been generated using different mesh discretizations of an increasing number of linear HEXA8 brick finite elements (HEXA8_1, HEXA8_2 and HEXA8_3, respectively, in Table 2). The distributions of longitudinal and transverse shear components of the stress field along the thickness of the fiber-matrix body are shown in Fig. 10. The solutions included correspond to the 3^{rd}, 6^{th} and 8^{th} polynomial expansions and the most refined Nastran model (HEXA8_3). In addition, the surface plots of those stress components are included in Fig. 11 for illustrative purposes. The results obtained in the present assessment suggest the following:

model	$u_z \times 10^5$ $[0, L, 0]$	$\sigma_{yy} \times 10^{-8}$ $[0, L/2, d/2]$	$\sigma_{yy} \times 10^{-8}$ $[0, L/2, 0.03]$	$\sigma_{yz} \times 10^{-5}$ $[-d/2, L/2, d/2]$	DOFs
MSC Nastran models					
$HEXA8_1$	-7.910	9.677	7.179	-3.798	47790
$HEXA8_2$	-7.879	9.626	7.148	-3.487	96300
$HEXA8_3$	-7.857	9.555	7.122	-3.394	296160
Classical and refined models based on TE [33]					
EBBT	-7.811	9.469	7.102	-1.962	363
TBT	-7.835	9.469	7.102	-1.962	605
N=1	-7.835	9.469	7.102	-1.962	1089
N=2	-7.774	9.358	7.019	-2.311	2178
N=3	-7.777	9.358	7.019	-2.464	3630
N=4	-7.794	9.327	7.090	-2.454	5445
N=5	-7.795	9.327	7.090	-2.375	7623
N=6	-7.800	9.315	7.105	-2.373	10164
N=7	-7.800	9.315	7.105	-2.304	13068
N=8	-7.804	9.346	7.117	-2.301	16335
LE models [33]					
12L9+8L6	-7.933	9.450	7.046	-2.500	7533
HLE models					
HL1	-0,459	0.100	0.073	1.903	744
HL2	-2.616	2.532	1.861	10.930	1860
HL3	-7.763	9.358	7.092	-3.224	2976
HL4	-7.771	9.400	7.071	-3.022	4557
HL5	-7.773	9.383	7.070	-2.997	6603
HL6	-7.774	9.412	7.080	-3.025	9114
HL7	-7.775	9.365	7.073	-3.445	12090
HL8	-7.775	9.361	7.071	-3.558	15531

Table 2: Displacements [m] and stress [Pa] solutions of the fiber-matrix beam at various points.

- According to the displacements results in Table 2, one can notice that, against of what one could expect, the solid models become stiffer when the mesh is refined. The reason is that the linear edges of the solid bricks are not adequate to represent the curved geometry of the fiber, and very fine discretizations are needed to evaluate properly its volume. This issue is eliminated in HLE models, since the geometry of the fiber is introduced as an input for the computation of the integrals of the problem. Obviously, the polynomial order of the cross-sectional expansions used for the fiber should be at least the same as the order of the mapping functions used to describe the geometry. This fact explains why the linear HL1 and quadratic HL2 models fail also for the computation of the primary solutions.

- HLE beam models show a remarkable performance in capturing the stress fields within the fiber-matrix body. The longitudinal stresses plotted in Fig. 10 (a) are almost on top the solid solutions for all polynomial orders considered. On the other hand, regarding the transverse shear stresses plotted in Fig. 10 (b), the HL3 model provides a quadratic distribution along the z-axis, which in this particular case is not enough to fulfill the equilibrium conditions at the interface of the fiber-matrix. Higher-order polynomial expansions overcome this issue, showing similar distributions as the solid model.

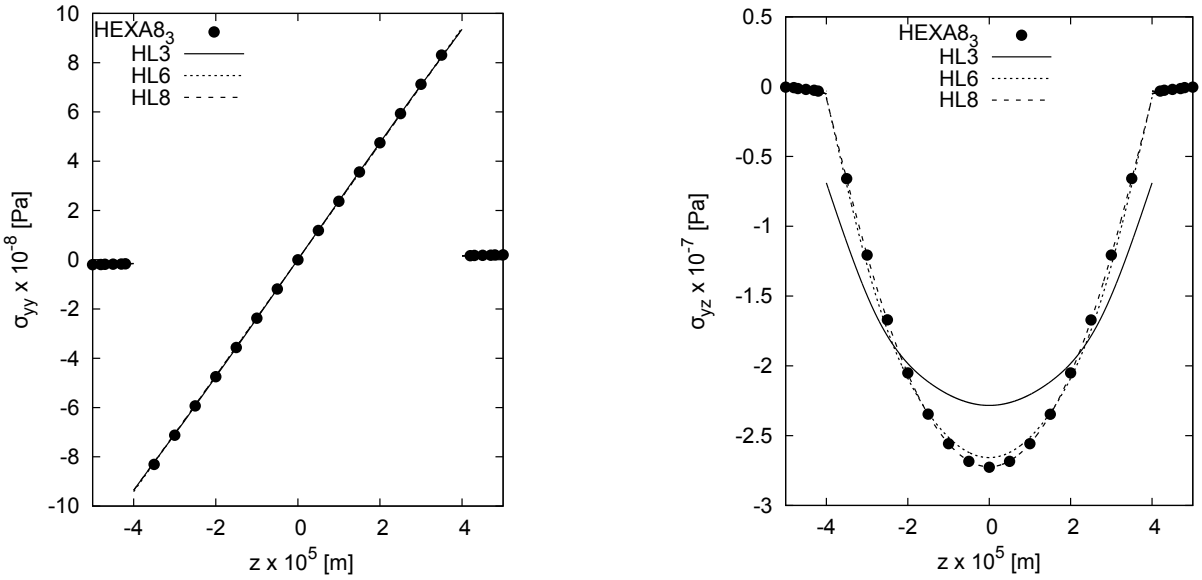

(a) σ_{yy} (b) σ_{yz}

Figure 10: Longitudinal and transverse shear stresses along the z-axis at [0,L/2,:].

In reality, a more complete understanding of the mechanics at the micro-scale of fiber-reinforced composites comes from having into account the interaction between the different components that are present in the material in form of clusters of fibers or tows. To obtain a more representative model of the micro-structure, an increasing number of fibers is usually accounted for the mechanical analysis. However, the huge computational costs required to capture in detail the heterogeneities at the fiber-scale remains as one of the main limitations

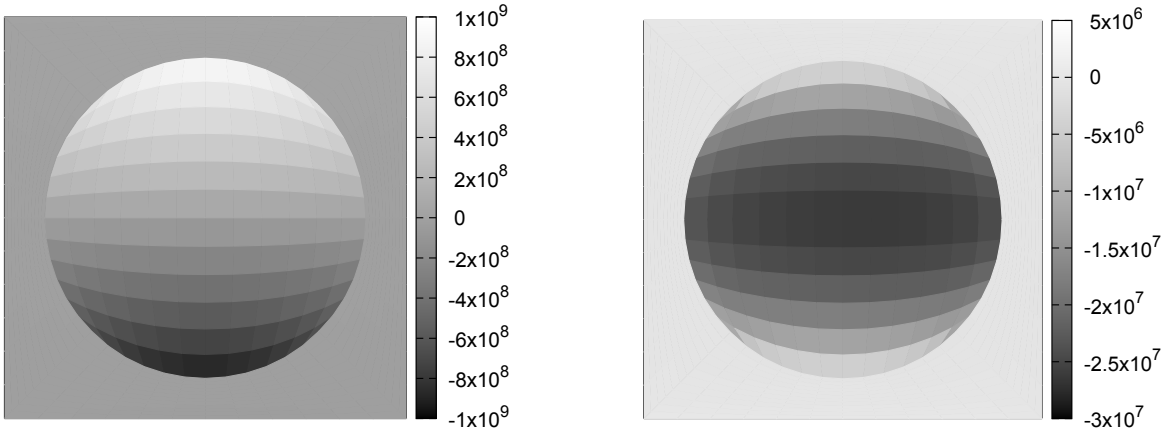

(a) σ_{yy} (b) σ_{yz}

Figure 11: Normal and transverse shear stress distributions [Pa] of the fiber-matrix beam at midspan, HL6 model.

of the multi-scale analysis. Following this direction and in order to show the potential of the present formulation in this matter, a double-fiber set is generated now by placing two fiber-matrix bodies, like the one considered in the previous analysis case, side-by-side along the x-axis, see Fig. 12. Again, each fiber is modeled using one single HLE mapped domain at the cross-sectional level and a 6^{th} order expansion is considered for the numerical solutions. In order to present a generic loading case, two forces are applied at the free-edge on different directions, as shown in Fig. 12, having both of them a magnitude of 1 N. As for the previous case, the structure is clamped at $y = 0$ and 10 cubic MITC beam elements are used for the longitudinal finite element mesh.

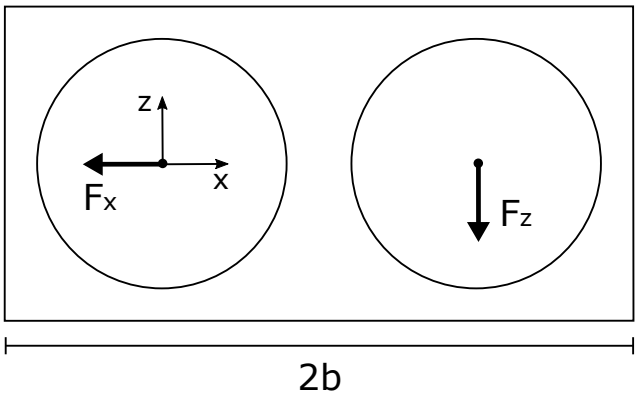

Figure 12: Cross-section of the double-fiber beam.

The numerical results of displacements and stresses are included in Table 3, and compared against those from a Nastran solid model. The accuracy of the proposed model for this structural case is undoubtedly equivalent to the solid model, although it requires only the 3.2 % of the number of degrees of freedom. The distribution of the relevant components of the stress field along the x-coordinate for these two models are plotted in Fig. 13 and 14. One can notice the good agreement of the solutions in all the cases considered. The

use of MITC high-order beam elements enhances the interpolation of the transverse shear components along the longitudinal axis and, therefore, the correct derivation of the integrals of the stiffness matrix, leading to a very accurate computation of the complete stress fields. Particularly interesting is the graph of Fig. 13 (b), which shows the σ_{xz} shear stresses at a section close to the loaded edge, $y = 0.9L$. HLE model solutions are sensible of the local effects due to the vertical point force, F_z, applied in the vicinity at [b, L, 0]. In fact, when a higher expansion order is employed (HL8), the local effects become more visible.

Model	$u_x \times 10^5$	$u_y \times 10^6$ [b, L, 0]	$u_z \times 10^4$	$\sigma_{yy} \times 10^{-8}$	$\sigma_{xy} \times 10^{-7}$ [b, L/2, 0]	$\sigma_{yz} \times 10^{-8}$	$\sigma_{xz} \times 10^{-7}$ [b/2, 0.9L, 0]	DOFs
MSC Nastran model								
HEXA8	-7.280	3.979	-3.973	8.346	-7.784	-1.375	-3.270	548550
HLE beam model								
HL6	-7.239	3.960	-3.925	8.308	-7.700	-1.340	-3.274	17577

Table 3: Results of displacements [m] and stresses [Pa] of the micro-scale fiber doublet.

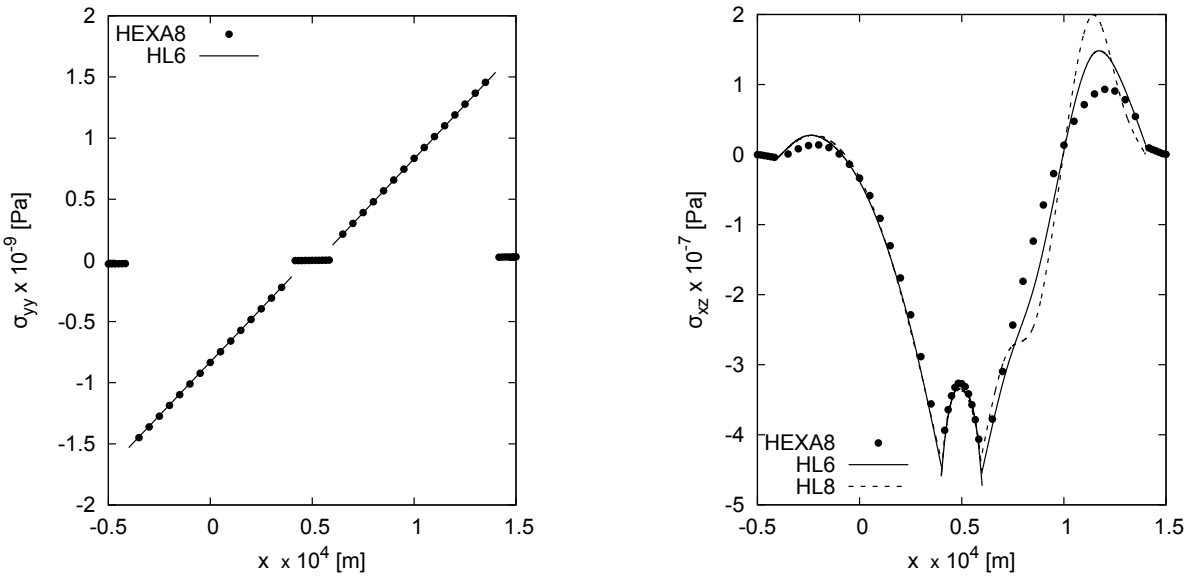

(a) σ_{yy} at $y = L/2$

(b) σ_{xz} at $y = 0.9L$

Figure 13: Longitudinal and in-plane shear stresses along the x-axis.

4.3 Cross-ply beam

For the last numerical assessment, a global-local analysis is carried out on a cross-ply laminated beam that includes fibers, matrix and homogenized layers as components. The Component-Wise method is employed here to locally select the level of accuracy of the stress analysis within the structural body. The geometry of the model is described in Fig. 15. The total length of the beam, L, is equal to 40 mm, the height, h is as high as 0.06 mm and the width, b, is equal to 0.08 mm. A symmetric cross-ply $[0°, 90°, 0°]$ is studied and a total of 4 fibers

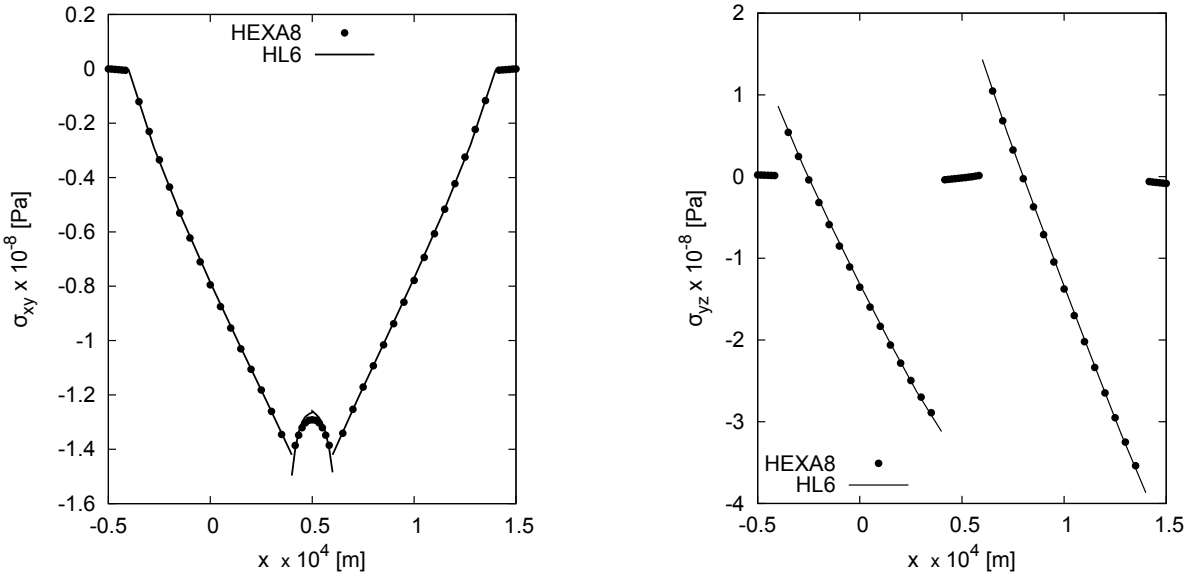

(a) σ_{xy} at $y = L/2$ (b) σ_{yz} at $y = L/2$

Figure 14: Transverse shear stress components along the x-axis.

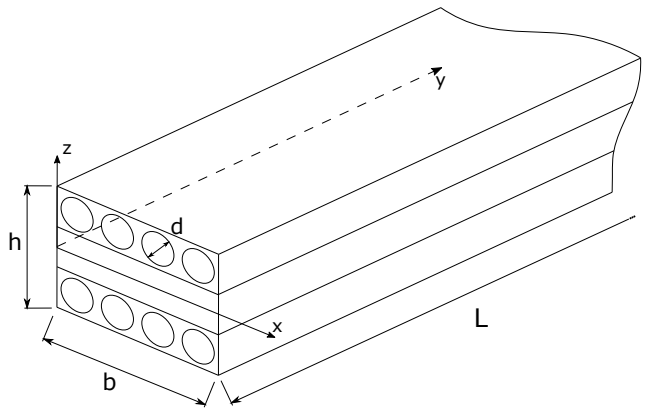

Figure 15: Geometry of the cross-ply beam.

Component	E_1	E_2	E_3	G_{12}	G_{13}	G_{23}	ν_{12}	ν_{13}	ν_{23}
Fiber	202.038	12.134	12.134	8.358	8.358	47.756	0.2128	0.2128	0.2704
Layer	103.173	5.145	5.145	2.107	2.107	2.353	0.2835	0.2835	0.3124
Matrix		3.252			1.200			0.355	

Table 4: 1 ≡ longitudinal, 2 ≡ orthogonal and 3 ≡ transverse.

are considered per layer, with a diameter of 0.016 mm each one. The mechanical properties of each component accounted in the analysis are presented in Table 4. The material of the fiber is considered as transversely isotropic, whereas the matrix is composed by an isotropic material. The engineering constants of the equivalent layer are calculated by means of the widely spread hybrid Rules of Mixtures. A clamped-free configuration is selected and a vertical point load of magnitude $F_z = -1$ N is applied at [b/2, L ,0] (see the coordinate frame in Fig. 15). Three different modeling approaches are considered for the structural analysis, which are:

1. HLE model 1. The cross-ply is analyzed in a layer-wise sense, i.e. the homogenized properties are used for the three layers. See Fig. 16 (a).

2. HLE model 2. The fiber-matrix cells are modeled for the top and bottom layers, whereas the homogenized properties are applied to the middle layer. See Fig. 16 (b).

3. HLE model 3. Only one single fiber-matrix cell of the bottom layer is modeled. See Fig. 16 (c).

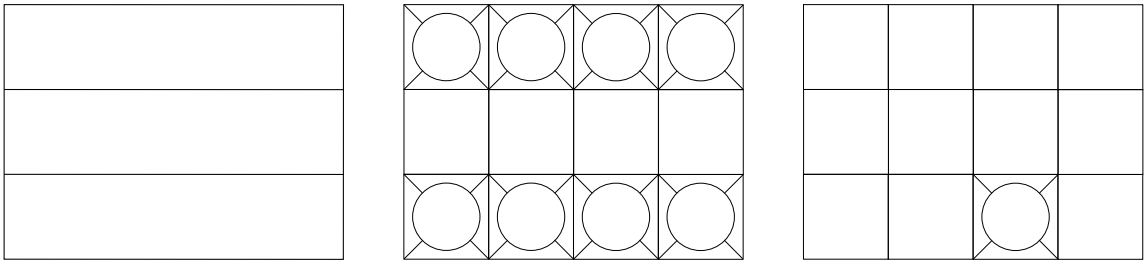

(a) HLE model 1 (b) HLE model 2 (c) HLE model 3

Figure 16: Cross-section domain distributions of the cross-ply beam

Table 5 presents the results in terms of displacement and stresses for all three approaches followed and for an increasing polynomial order of the HLE expansions. A Nastran 3D model with the geometry and properties of the second approach (model 2) has been generated and its results are displayed as reference solutions. The vertical displacement is measured at the loading point, whereas the longitudinal and transverse stresses are evaluated at the position of the center of the fiber accounted in model 3 (see Fig. 16 (c)), at the midspan section. The distribution of these components across the thickness at that location are shown in Fig. 17 for all three refined beam models and the solid one used as reference. In addition, Figs. 18 and

19 show an interesting comparison of the stress distributions over the cross-section obtained with the HL6 model for the three modeling approaches considered. The main conclusions of the present numerical example are:

- The numerical values of Table 5 exhibit a general good agreement of the HLE solutions in comparison with the Nastran model. Displacements solutions are less dependent on the choice of the modeling approach than stress solutions, although they slightly diverge from the reference solutions when global approaches are employed due to the simplifications introduced when the fiber-matrix set is homogenized.

- The HL2 model provide good solutions for the layer-wise approach, although it should be avoided when higher-order mapped expansions are included. It is possible to state that at least a third-order HL3 model must be employed for mapped domains.

- The use of solid brick elements for this type of multi-component structures can become highly expensive if a detailed mechanical analysis is required at the component level. HLE mapped models naturally overcome some of the constrains of solid modeling, such as the aspect ratio or the geometrical accuracy of the mesh, for structural problems featuring 2D heterogeneities. In this example, the maximum relative difference between the numerical values of model 2 and the Nastran model remain in all cases under 3.5 % (HL2 excluded), while keeping the number of degrees of freedom less than 5 % of those of the solid model.

- The main advantage of the Component-Wise approach for the efficient stress analysis of composite materials is that it allows to enrich the kinematics of the beam model in particular zones of interest. The efficiency of the modeling procedure can be greatly enhanced taking advantage of these capabilities of the CUF. For instance, one can see in Fig. 17 that the layer-wise approach (model 1), although computationally very advantageous, fails on predicting the maximum stresses of the structure, whereas model 2 and 3 provide a 3D-like accuracy at the fiber-matrix level with acceptable increments in computational costs. This statement is further supported by the stress distributions shown in Fig. 18 and 19.

5 Conclusions

This paper presents the application of HLE beam theories with advanced mapping capabilities for the accurate analysis of composite structures that include components with arbitrary curved sections. The Carrera Unified Formulation is employed to generate a class of refined beam elements that make use of hierarchical Legendre-based polynomials to expand the mechanical variables non-locally over the cross-section domain. Laminates and fiber-reinforced bodies are analyzed and the results are compared with those from solid models generated

	$u_z \times 10^2$ m [b/2, L, 0]	$\sigma_{yy} \times 10^{-8}$ Pa [5b/2, L/2, -0.2]	$\sigma_{yz} \times 10^{-6}$ Pa [5b/2, L/2, -0.2]	DOFs
		MSC Nastran model		
HEXA8	-1.569	-5.928	-2.147	1579653
		HLE model 1		
HL2	-1.491	-2.880	-1.577	4743
HL3	-1.491	-2.880	-1.710	7626
HL4	-1.491	-2.879	-1.712	11625
HL5	-1.491	-2.879	-1.655	16740
HL6	-1.491	-2.880	-1.654	22971
		HLE model 2		
HL2	-0.348	-0.838	-43.008	13671
HL3	-1.547	-5.849	-2.142	22506
HL4	-1.548	-5.848	-2.169	35433
HL5	-1.548	-5.848	-2.211	52452
HL6	-1.548	-5.848	-2.212	73563
		HLE model 3		
HL2	-1.046	-3.717	-124.390	5859
HL3	-1.498	-5.661	-2.384	9486
HL4	-1.498	-5.659	-2.381	14601
HL5	-1.498	-5.659	-2.412	21204
HL6	-1.498	-5.659	-2.408	29295

Table 5: Displacements and stresses of the cross-ply beam for the different models.

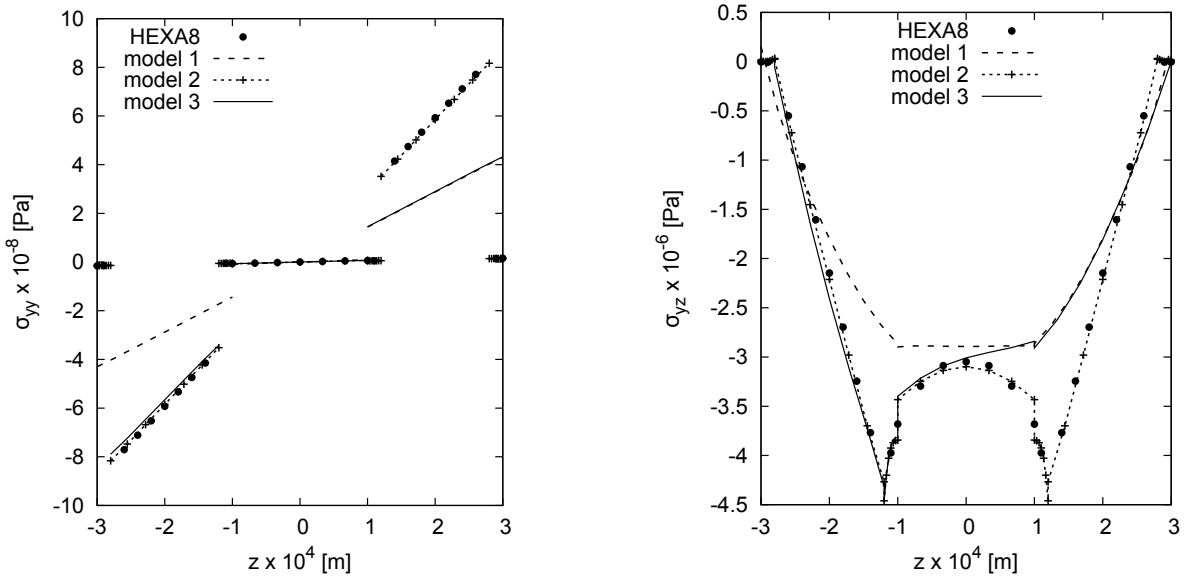

(a) σ_{yy} (b) σ_{yz}

Figure 17: Longitudinal and shear stresses across the thickness of the section at [5b/2,L/2,:] for all the approaches considered. HL6 expansion.

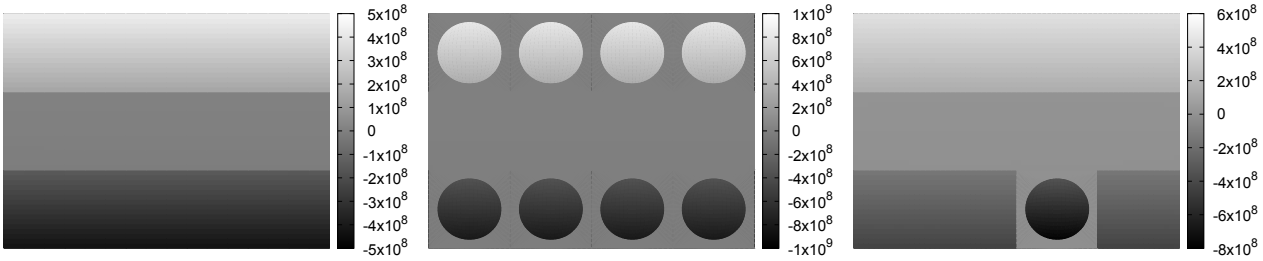

(a) model 1 (b) model 2 (c) model 3

Figure 18: Normal stress distribution at midspan of the cross-ply for the different models considered. HL6 expansion.

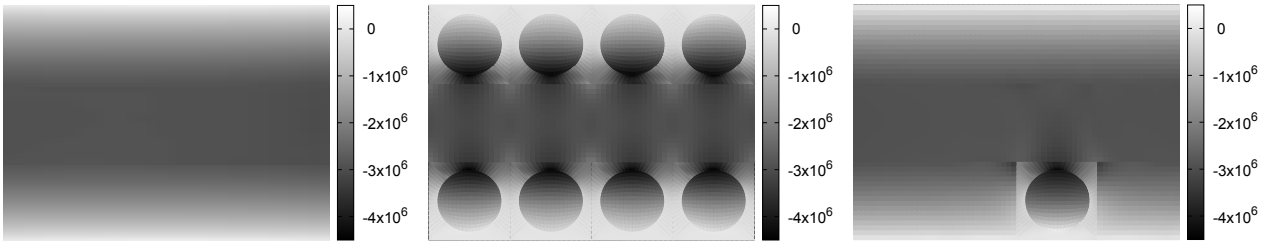

(a) model 1 (b) model 2 (c) model 3

Figure 19: Transverse shear stress distribution at midspan of the cross-ply for the different models considered. HL6 expansion.

with the commercial software Nastran and the literature, when possible. On the basis of the results obtained, the following comments can be highlighted:

- The HLE beam formulation can be used to provide advanced layer-wise models for the study of laminated structures. The use of the blending function method to curve the expansion domains at the cross-sectional level leads to a more efficient analysis in which the geometrical description is fixed and the accuracy of the model is controlled by the polynomial order of the theory of structure, in a non iso-parametric sense.

- HLE beam models have demonstrated to be a powerful tool for the Component-Wise analysis of composite structures. The kinematics of the structural model can be enriched locally in critical zones within the cross-section in a hierarchical manner with no need of further refinements of the physical description of the body, which can lead to huge savings in the modeling time.

- The potential of the proposed model for the structural analysis of fiber-reinforced composites at the micro-scale is clear. The HLE models can deal with the complex stress fields that appear at the fiber-matrix level for general loading cases with the same accuracy as solid models, while reducing drastically the size of the computational problem.

The results obtained in this work provide a good basis for further analysis of more complex models dealing with other realistic cases of interest, such as clusters of randomly place fibers

or different fiber sections, which is currently one of the major concern in micro-mechanics and multi-scale analyses.

Acknowledgements

This research has been carried out within the project FULLCOMP – FULLy analysis, design, manufacturing, and health monitoring of COMPosite structures – funded by the Marie Sklodowska-Curie actions grant agreement no. 642121. The H2020 European Training Networks are gratefully acknowledged.

References

[1] J. N. Reddy. *Mechanics of laminated composite plates and shells. Theory and Analysis*. CRC Press, 2^{nd} edition, 2004.

[2] R.K. Kapania and S. Raciti. Recent advances in analysis of laminated beams and plates, part I: Shear effects and buckling. *AIAA Journal*, 27(7):923–935, 1989.

[3] R.K. Kapania and S. Raciti. Recent advances in analysis of laminated beams and plates, part II: Vibrations and wave propagation. *AIAA Journal*, 27(7):935–946, 1989.

[4] T. Kant, D.R.J. Owen, and O.C. Zienkiewicz. A refined higher-order C° plate bending element. *Computers & Structures*, 15(2):177 – 183, 1982.

[5] B.N. Pandya and T. Kant. Higher-order shear deformable theories for flexure of sandwich plates. Finite element evaluations. *International Journal of Solids and Structures*, 24(12):1267 – 1286, 1988.

[6] M. Touratier. An efficient standard plate theory. *International Journal of Engineering Science*, 29(8):901 – 916, 1991.

[7] J. N. Reddy. A simple higher-order theory for laminated composites. *Journal of Applied Mechanics*, 51:745–752, 1986.

[8] H. Matsunaga. Interlaminar stress analysis of laminated composite beams according to global higher-order deformation theories. *Composite Strucutures*, 55:105–114, 2002.

[9] E. Carrera and G. Giunta. Refined beam theories based on Carrera's unified formulation. *International Journal of Applied Mechanics*, 2(1):117–143, 2010.

[10] A.J.M. Ferreira, C.M.C. Roque, and R.M.N. Jorge. Analysis of composite plates by trigonometric shear deformation theory and multiquadrics. *Computers & Structures*, 83(27):2225 – 2237, 2005.

[11] S.G. Lekhnitskii. Strength calculation of composite beams. *Vestnik inzhen i tekhnikov*. No 9.

[12] H. Arya, R.P. Shimpi, and N.K. Naik. A zigzag model for laminated composite beams. *Composite Structures*, 56(1):21 – 24, 2002.

[13] E. Carrera. Historical review of zig-zag theories for multilayered plates and shells. *Applied Mechanics Reviews*, 56(3):287–308, 2003.

[14] P. Vidal and O. Polit. A sine finite element using a zig-zag function for the analysis of laminated composite beams. *Composites*, 43:1671–1682, 2011.

[15] E. Reissner. On a mixed variational theorem and on shear deformable plate theory. *International Journal for Numerical Methods in Engineering*, 23(2):193–198, 1986.

[16] M.K. Rao, Y. Desai, and M. Chistnis. Free vibrations of laminated beams using mixed theory. *Composite Structures*, 52:149–160, 2001.

[17] J. N. Reddy. On refined computational models of composite laminates. *International Journal for Numerical Methods in Engineering*, 27(2):361–382, 1989.

[18] R.P. Shimpi and Y.M. Ghugal. A new layerwise trigonometric shear deformation theory for two-layered cross-ply beams. *Composites Science and Technology*, 61(9):1271 – 1283, 2001.

[19] N.J. Pagano. Exact solutions for composite laminates in cylindrical bending. *Journal of Composite Materials*, 3(3):398–411, 1969.

[20] K. Surana and S. Nguyen. Two-dimensional curved beam element with higher-order hierarchical transverse approximation for laminated composites. *Computers and Structures*, 36:499–511, 1990.

[21] M. Tahani. Analysis of laminated composite beams using layerwise displacement theories. *Composite Structures*, 79(4):535 – 547, 2007.

[22] D.H. Li, Y. Liu, and X. Zhang. An extended layerwise method for composite laminated beams with multiple delaminations and matrix cracks. *International Journal for Numerical Methods in Engineering*, 101(6):407–434, 2015.

[23] E. Carrera and M. Petrolo. Refined one-dimensional formulations for laminated structure analysis. *AIAA Journal*, 50(1):176–189, 2012.

[24] R. Hill. Theory of mechanical properties of fibre-strengthened materialsIII. self-consistent model. *Journal of the Mechanics and Physics of Solids*, 13(4):189 – 198, 1965.

[25] J. Aboudi. A continuum theory for fiber-reinforced elastic-viscoplastic composites. *International Journal of Engineering Science*, 20(5):605 – 621, 1982.

[26] M. Paley and J. Aboudi. Micromechanical analysis of composites by the generalized cells model. *Mechanics of Materials*, 14(2):127 – 139, 1992.

[27] E. Pineda and A. Waas. Multiscale failure analysis of laminated composite panels subjected to blast loading using feamac/explicit. *NASA/TM, 2009215813*, 2009.

[28] A. Bensoussan, J. Lions, and G. Papanicolaou. *Asymptotic Analysis for Periodic Structures*. North-Holland, 1978.

[29] C.T. Sun and R.S. Vaidya. Prediction of composite properties from a representative volume element. *Composites Science and Technology*, 56(2):171 – 179, 1996.

[30] T. Kanit, S. Forest, I. Galliet, V. Mounoury, and D. Jeulin. Determination of the size of the representative volume element for random composites: statistical and numerical approach. *International Journal of Solids and Structures*, 40(1314):3647 – 3679, 2003.

[31] S. Ghosh and D. V Kubair. Exterior statistics based boundary conditions for representative volume elements of elastic composites. *Journal of the Mechanics and Physics of Solids*, 95:1–24, 2016.

[32] W. Yu. A unified theory for constitutive modeling of composites. *Journal of Mechanics of Materials and Structures*, 11(4):379–411, 2016.

[33] E. Carrera, M. Maiarù, and M. Petrolo. Component-wise analysis of laminated anisotropic composites. *International Journal of Solids and Structures*, 49:1839–1851, 2012.

[34] E. Carrera, A. Pagani, and M. Petrolo. Component-wise method applied to vibration of wing structures. *Journal of Applied Mechanics*, 80(4):041012, 2013.

[35] E. Carrera, A. Pagani, and M. Petrolo. Classical, refined, and component-wise analysis of reinforced-shell wing structures. *AIAA Journal*, 51(5):1255–1268, 2013.

[36] E. Carrera and A. Pagani. Free vibration analysis of civil engineering structures by component-wise models. *Journal of Sound and Vibration*, 333(19):4597–4620, 2014.

[37] M. Maiarù, M. Petrolo, and E. Carrera. Evaluation of energy and failure parameters in composite structures via a component-wise approach. *Composites Part B*, 108:53–64, 2017.

[38] E. Carrera, A.G. de Miguel, and A. Pagani. Hierarchical theories of structures based on Legendre polynomial expansions with finite element applications. *International Journal of Mechanical Sciences*, (120):286–300, 2017.

[39] A. Pagani, A.G. de Miguel, M. Petrolo, and E. Carrera. Analysis of laminated beams via unified formulation and Legendre polynomial expansions. *Composite Structures*, pages –, 2016. In Press.

[40] A. Pagani, A.G. de Miguel, and E. Carrera. Cross-sectional mapping for refned beam elements with applications to shell-like structures. 2017. Submitted.

[41] E. Carrera and M. Petrolo. Refined beam elements with only displacement variables and plate/shell capabilities. *Meccanica*, 47(3):537–556, 2012.

[42] B. Szabó and I. Babuska. *Finite Element Analysis*. John Wiley and Sons, Ltd, 1991.

[43] W.J. Gordon and C.A. Hall. Transfinite element methods: Blending-function interpolation over arbitrary curved element domains. *Numerische Mathematik*, 21(2):109–129, 1973.

[44] M. Petrolo E. Carrera, G. Giunta. *Beam structures: classical and advanced theories*. John Wiley and Sons, 2011.

[45] O. C. Zienkiewicz, R. L. Taylor, and J. M. Too. Reduced integration technique in general analysis of plates and shells. *International Journal for Numerical Methods in Engineering*, 3(2):275–290, 1971.

[46] T.J.R. Hughes, M. Cohen, and M. Haroun. Reduced and selective integration techniques in the finite element analysis of plates. *Nuclear Engineering and Design*, 46(1):203 – 222, 1978.

[47] E.N. Dvorkin and K.J. Bathe. A continuum mechanics based four-node shell element for general non-linear analysis. *Engineering Computations*, 1(1):77–88, 1984.

[48] R.H. MacNeal. Derivation of element stiffness matrices by assumed strain distributions. *Nuclear Engineering and Design*, 70(1):3 – 12, 1982.

[49] E. Carrera, A.G. de Miguel, and A. Pagani. Extension of MITC to higher-order beam models and shear locking analysis for compact, thin-walled and composite structures. 2017. Submitted.

[50] E. Carrera, M. Cinefra, E. Zappino, and M. Petrolo. *Finite Element Analysis of Structures Through Unified Formulation*. John Wiley and Sons, Ltd, 2014.

[51] MSC.Software Corporation. MD Nastran 2010 Quick Reference Guide. 2010.